SLM Materials Development

A Senior Project submitted to

the Faculty of California Polytechnic State University,

San Luis Obispo

In Partial Fulfillment

of the Requirements for the Degree of

Bachelor of Science in Manufacturing Engineering

by

Justin Reiner & Michael Schembri

June 12, 2018

ABSTRACT

SLM MATERIALS DEVELOPMENT

Justin Reiner & Michael Schembri

The purpose of this project was to create a procedure to efficiently determine a “recipe” of parameter values that create a desired set of mechanical properties. Research was conducted into the laser powder bed fusion process with focus on underdeveloped materials. A design of experiment was used with a set of density correlated parameters to establish a method of producing nearly dense parts. Our methods include SLM printing, metrology, and statistical analysis. An experimental procedure for materials development was designed, but unable to be validated during the scope of this project, due to unforeseen safety issues (exposure to Chromium 6, a toxic substance). Next steps include validation of this procedure using various metal powders in a SLM 125 HL.

ACKNOWLEDGMENTS

We would like to acknowledge the following people for their aid in our senior project:

Special thanks to Dr. Xuan Wang for his continued assistance and expert advice throughout both quarters of this project.

Special thanks to Dr. Daniel Waldorf for his advice on the direction of this project.

Special thanks to Trian Georgeou for his technical assistance.

Special thanks to Martin Koch for assisting Dr. Wang in updating safety procedures for the SLM printers at Cal Poly.

Special thanks to Jeffrey Zimmerman for his assistance with design of experiments.

TABLE OF CONTENTS

LIST OF TABLES

Table Page

LIST OF FIGURES

Figure Page

I. Introduction

Selective Laser Melting (SLM) is an additive manufacturing process used to melt metal powder using a powerful laser. Additive manufacturing, laser powder bed fusion specifically, has proven to be an efficient and economically viable form of rapid prototyping and manufacturing. Fairly recently, new materials have been tested on SLM outside of 316L Stainless Steel. This report will focus on research using Glenn Research Copper-84 as the case study for general materials development. Our objectives for a successful ‘recipe’ of parameters is to yield a part of 99% density within 4 builds of 16 parts each, to minimize warpage in bigger parts, and to determine the parameters that positively affect surface finish, dimensional accuracy, and durable mechanical properties. The recipe yielded by the experiment will also give values for optimizing residual stresses, porosity, and tensile strength.

II. Literature Review

GRCop-84: A High-Temperature Copper Alloy for High-Heat-Flux Applications Glen research copper 84 was created to fulfill the need for a copper based alloy with multiple specific properties. These properties would be that the alloy needed to have excellent elevated temperature strength, good creep resistance, long low-cycle fatigue lives, as well as enhanced oxidation resistance. Copper alloys of this nature need to be produced using advanced production techniques (rapid solidification technology) due to the fact that Cr_2Nb precipitates, causing it to grow to more than 1 cm in diameter during slow cooling. The specific rapid solidification technology used with this alloy with high success is conventional argon gas atomization. It was chosen for its large industrial base, low cost, production volume abilities, and high cooling rate. The alloy is also produced in fine powder forms, which can be used for extrusion and hot isostatic pressing. A finer powder is made for manufacturing methods such as vacuum plasma spraying, as well as additive manufacturing. After the raw metal is produced, it can be processed in many different traditional ways of forming, rolling, drawing, etc. The microstructure of the alloy shows a high volume of Cr_2Nb, approximately 14% by volume. This intermetallic compound dispersion strengthens the copper matrix, giving the alloy its desirable properties that NASA seeks in the new generation of Main Combustion Chamber Liners.

Comparison of GRCop-84 to Other Cu Alloys With High Thermal Conductivities GRCop-84 as a recently created copper alloy needs to prove itself against what was available at the time of its creation for production. It is often compared to: AMZIRC, GlidCop Al-15, Cu-1Cr-0.1Zr, Cu-0.9Cr, and NARloy-Z. The alloys were compared in a multiple of ways: tensile, compressive, creep, thermal expansion, and with low cycle fatigue lives. The alloys were received in their respective production methods. GrCop-84 was extruded and HIPed, while the other alloys were produced in the form of hard drawn rods. The alloys all went through a brazing process meant to replicate the normal operation in the main combustion chamber liner. All of the alloys, except for GrCop, were stronger in tension and compression when less than 500 degrees Celsius. After the simulated brazing operation, GRCop-84 and GlidCop Al -15 are stronger than all other alloys. After these alloys were brazed, they had higher temperature creep than the remaining alloys. The defining feature between GRCop-84 and GlidCop Al -15 is that GrCop-84 has better ductility and processing characteristics.

Creep properties of an extruded copper–8% chromium–4% niobium alloy Creep resistance is an extremely useful mechanical property of materiale in many engineering applications. It is a defining property of GrCop-84 due to its fine grained copper matrix that contains particulate amounts of Cr_2Nb. GRCop-84 was made in two stages pre production and production. The production and pre production GRCop-84 were manufactured via extrusion and rolling. It was observed that the mechanical properties of the two stages rivaled each other producing no defining differences in testing. The microstructure of GRCop-84 is seen to

correlate to its creep properties. GRCop-84 show tensile ductility that exceeds of 10% true strain at creep temperatures as well exceeds 13% engineering strain at room temperature. These observations were show that GRCop-84 fails testing because of void growth and coalescence together with extensive creep crack growth and interlinkage.

Improvement of GRCop-84 Through the Addition of Zirconium

GRCop-84, an already impressive copper alloy, has a microstructure that contains Cr_2Nb particles and a near pure copper matrix. This allows the copper to have its key properties of great creep resistance, low cycle fatigue life, and the ability to maintain these at high heats. It has been seen that adding zirconium to other copper alloys has helped to improve upon these alloys' strengths. With Zirconium being added to GRCop-84, it will be tested in a multitude of ways to see how it compares to standard GRCop-84's properties. the addition of Zr to GRCop-84 produced increased the tensile strength at room temperature and 500 degrees celsius. It was also seen that the creep resistance was also positively affected at room and 500 degrees celsius. Low cycle fatigue life was not necessarily affected by the addition of Zr. In conclusion GRCop-84 can benefit from the addition of Zr and its effects should be realized.

Economics of additive manufacturing for end-usable metal parts

Additive manufacturing allows there to be a completely different set rules for when designing parts, when compared to traditional (non-AM) methods. This is addressed with design for manufacturing (DFM) rules for additive manufacturing. Due to its unique capabilities, AM processes allow the design of undercuts in parts as well as the ability for varying wall thickness in parts. This allows for parts of extreme complexity to be able to be produced. Also, the use of support structures during the building, several parts can be integrated into each other allowing them to be built in one operation. Comparing the costs of manufacturing between a complex part made with high pressure die casting and one made with selective laser sintering, the additive manufactured part will cost less. Also, with selective laser sintering, the three part assembly can be made as one part, functioning just as well or even better due to the part being lighter in weight. As well, the cost analysis proving that unless the manufacturer were producing more than 50 parts, using AM costs less than using specialty traditional manufacturing.

Environmental and Economic Implications of Distributed Additive Manufacturing

Additive manufacturing has enabled manufacturers to create parts with superior engineering functionality as well as greatly speeding up supply chains, and creating parts that are sustainable in many ways. by the use of an integrate techno economic model to estimate the effects that AM has on lead time, life cycle, costs comparison against injection molding, and effects on greenhouse gases. the results of this estimate show that there was a potential savings on lead time between 12-60%, a 70-80% saving on downtime, a 3-5% saving on overall energy usage, 4-7% saving on amount of GHG emissions, and most importantly a 15-35% saving on cost compared

to injection molding. All these results were done as a direct comparison to one million cycles of injection molding.

Economic implications of 3D printing: Market structure models in light of additive manufacturing revisited

Additive manufacturing is bringing a spark to manufacturing as a whole. making it so parts that were too complex to be manufactured traditionally can manufactured by AM. Thus allowing creativity to burst out of the seams and new products and inventions to be made. As well it allows part to be made much more economically because of no need for specialty tooling. AM adds value for producers and customers in the way that it can be used for for prototyping so that cost of product development can be greatly reduced. AM adds a significant amount of value to manufacturing because it can offer customization without extreme effects on cost. As well AM can greatly reduce the costs of assembly steps in manufacturing because of the ability to create integrated parts that would previously require an assembly step. All of these and more advantages show the advantages of additive manufacturing and the value that it will add when it is fully integrated in the future.

Tools for Sustainable Product Design: Additive Manufacturing

The creation of additive manufacturing and its recent gain of popularity have created a new alleyway for designers and manufactures that have helped to extend parts sustainability. It can be seen this way in that a part that is designed and manufactured very well could create desirability and pleasure and create an attachment to a well designed item. This really ties to additive manufacturing because it can be customizable in mass because of no need to create tooling to customize parts. This directly correlates to sustainability because a part that is customized for a customer they are more likely to keep for an extended period of time. Another factor of sustainability for AM is the freedom of design because AM essentially eliminates all restrictions of traditional manufacturing technology and complex parts can be produced much more economically.

The Influence of Selective Laser Melting Parameters on Density and Mechanical Properties of AlSi10Mg

Aluminum silicon alloys are a very high strength aluminum alloy. They are very light and have great corrosion resistance, making them a desirable metal to make parts across multiple industries. Also, this makes it desirable for the parts to be produced using additive manufacturing, since it allows complex geometries to be produced. The parameters used to develop this material on the SLM machine are those of: Laser Power, Scanning speed, and hatching distance. These parameters were changed in a row matrix format of test blocks changing one parameter per row. It was found that these parameters had effects on the density of

the cubes. The parameter that had the best density percentages was scan speed when it was varied.

The Effects of Processing Parameters on Defect Regularity in Ti-6Al-4V Parts Fabricated By Selective Laser Melting and Electron Beam Melting

In laser powder bed additive manufacturing two technologies that are being used to successfully manufacture parts of metallic material. These technologies are that of electron beam melting (EBM) and selective laser melting(SLM). A SLM machine will use a fiber laser to selectively melt very thin layers of powder that will form a solid part. the EBM machine is similar to this but instead of a fiber laser it uses an electron beam generated via a a tungsten filament. The two technologies were compared by adjusting defined parameters with Ti-6Al-4V. The parameters that were adjusted with SLM were laser power(W) and scanning speed. The parameters that were changed with EBM were those of: max current, line offset, focus offset, and the speed function index. It is seen that the the adjustment of these parameters affects how much energy is in the build. It was seen that the energy density in the build did not correlate to porosity in builds. The marginal parameters are what are responsible for defect generation. For example in the SLM process splashed particles are welded out of position and the recoater breaks these off creating porosities.

Printing of CuCrZr Parts

Laser powder bed fusion has been successfully used to print dense parts with CuCrZr. “Using remelting at a layer-thickness of 20 μm, a maximum laser-power of 370W and 300 mms^{-1} scan speed a bulk density of 99.96% can be attained.” (Buchmayr). Buchmayr *et al* found that parts that underwent remelting had significantly higher density than those that did not. However, 99.1% +-1% density was still achievable with a single melt scan pattern. Layer thickness has to be adjusted to the melt pool depth to ensure proper bonding and high density. Heat treatment post print is needed to increase thermal conductivity and hardness.

Categories of Part Defects from LPBF Process

Porosity is a critical defect in metal AM parts as it severely affects the fatigue performance of the part. Porosity appears as voids that can appear within a layer, between layers, or on the surface of the part.

Residual stresses result from the thermal gradient that is created by the movement of the laser and the cool-down phase of layers. Residual stresses can result in delamination or cracks. Cracks occur when the cooling layer pulls on the layer below with more force than the ultimate tensile strength of the material. Delamination is a special case where the cracking propagates between adjacent layers of the build. When the molten material solidifies into individual balls rather than

into a continuous layer, it is referred to as melt ball formation, or balling. Surface tension is behind this phenomenon, as is prevents the molten material from wetting to the layer below.

Geometric defects and dimensional inaccuracies most commonly appear as shrinkage and warping. A particular combination of shrinkage and warping called curling affects downward faces meant to be flat by yielding a curved profile. Another severe defect is super-elevated edges. This occurs at the edges of the part and results in deterioration of the surface and dimensional accuracy of the part.

Surface defects mainly occur due to the layer-by-layer nature of the selective laser melting process. The surface finish is dependent on build orientation, upward and downward faces have considerably better surface finish than the side faces. Surface defects can also be caused balling or porosity.

Microstructural inhomogeneities arise due to the highly localized heat input of either the laser or the electron beam. Microstructural inhomogeneities have detrimental effects on the mechanical and functional performance of an AM part. Types of inhomogeneities include impurities, grain size characteristics and crystallographic textures. These defects often occur due to metal powder contamination or the presence of unmelted metal powder in the finished part.

In-Situ Monitoring of LPBF Process

Process phenomena such as spatter, plume formation, laser modulation, and melt-pool oscillations require data collection to occur at rates of 10 kHz or higher. This limits the real time monitoring and feedback systems that can be used.

Four single point sensors were experimented on as synchronized in-situ data acquisition devices, a thermal camera, a high speed visible camera, a photodiode, and laser modulation signal. The thermal camera provides temperature data, the visible camera provides spatter data, the photodiode signal was analyzed using joint-time frequency analysis. The images are woven together to allow for visual comparison of phenomena from the photodiode signal with the images from the cameras.

The experiment identified a strong relationship between photodetector signal and the location and motion of the melt pool. Two hypothesis were generated from the results of this experiment, “signal content is increased by the existence of spatter particle reflections on a solidified surface, and overall signal increases when the melt pool nears the overhang due to likely increases in melt pool size, temperature, and spatter frequency, and this effect is a greater contributor to overall signal levels.” (Lane).

Modelling and Simulation of LPBF Process

With the increasing use of AM, there is an increased need to create accurate models and simulations of the LPBF process. A modelling strategy would serve as the foundation for process control and part qualification. Lawrence Livermore Laboratories has presented a multiscale strategy for modelling this process, starting at the powder level simulating laser movement and provides powder bed and melt pool data. A second model computationally builds the complete part to predict properties such as residual stress and dimensional accuracy. Data mining methods attached to both of these models to optimize the AM process. The effective medium model, as LLL calls it, demonstrated a strategy for mitigation of dross formation on overhang features, as well as accurately predict residual stresses in a 6 cm tall prism part. Simulation was uniquely useful in narrowing the range of parameters to be investigated with experimentation. This ultimately reduces experimental costs through reduction of trials needed. An unintended byproduct of this simulation experiment was the agreement with a previous observation that the range of speeds over which near full density is obtained widens with the increase of laser power.

SLM for Magnetic Materials

A study was conducted by the National Cheng Kung University to see which SLM process parameters have the largest effect on the magnetic properties of the part by analyzing the magnitude of the magnetic properties in comparison with process parameters. The study found that for a powder that is 33.78um and shaped spherically, efficiency is maximized when laser power is 170W and scan speed is 950 nm/s. Oxygen content in the chamber should be kept below 5%. With these parameters, it was found that the magnetic property of a sintered ring of FeSiCr alloy is better than traditional silicon steel.

Multi-Structured Ti-6Al-7Nb Implants

The purpose of the study was to present how customized implants could be made with specific porosity by setting different values of laser power on the SLM machine. For implants, a significant amount of porosity is required for the material to mirror the properties of bone. Using laser powers ranging from 50 to 200 W, the studies found that structures had an open porosity ranging from 24.81% to 0.83%. Pore size range varied from 70-100μm to 200-400μm. The larger values facilitate tissue perpetration throughout the implant. For low laser powers, the Young's moduli of the material matches that of surrounding bone. By surrounding the prosthesis in a layer of porous material, bone growth is facilitated. Beyond the possibilities for prosthetics and implants, this study presents the a strategy for varying the parameter laser power in different areas of the build to produce desired properties in respective areas of the part.

Review of selective laser melting: Materials and applications

Selective laser melting is an additive manufacturing (AM) process that uses a high power density laser or beam to selectively melt and fuse metallic powder within and between layers. This

technique is capable of producing near net shape parts with 99.9% density. The further development of AM technology will continue to make this technique economically viable. Further development has also allowed this process to be used on more materials, such as copper, aluminum, and tungsten. Research is currently trending towards the use of SLM for ceramics and composite materials.

An Integrated Cost-Model for Selective Laser Melting

Due to the increased integration of AM processes into production environments, Rickenbacher developed a cost model capable of calculating costs for each part on a mixed job build plate while also including all pre- and post-processing steps. The model is adapted from the generic cost model of Alexander *et al.* The study found that simultaneously building multiple parts cost can be reduced by an average of 41% due to the reduction of setup time and the increase in throughput. The models cost algorithms enables precise determination of total cost per part even with extremely complex part geometries. This allows parts to be pooled across jobs, while maintaining cost accuracy. This allows for better optimization of build volume by suggesting aggregating parts of similar heights on the same build plate.

Selective Laser Melting of Copper Using Ultrashort Laser Pulses

The application of ultrashort pulse lasers for SLM is a recent trend. These systems provide high peak power and the potential to control the thermal impact in the vicinity of the processed region by adjusting the pulse repetition rate. The application of this system is useful for materials with extremely high melting points such as tungsten or special composites. A parameter study was conducted by Kaden *et al* using an ultrashort pulse laser on copper. The thermal conductivity of copper poses a great challenge in using the material in AM when resolutions below a micrometer. The study found that heat accumulation from the using high pulse repetition rates is able to melt the powder before the heat can dissipate into the bulk material. The focal spot size also has a significant impact on the melt pool. Using ultrashort pulse lasers narrows the active heating zone enabling for the fabrication of intricate 3D geometries that could be useful in microelectronic applications. However, the small focal spot leads to higher porosity, therefore if density is key, a larger focal spot size should be utilized. Scan speed can be increased only so far as the available laser power can be provided. Using ultrashort pulse-induced melting, solid cuboids and thin-wall structures with thicknesses of 100μm could be produced. These parts have high porosity due to the fact that the size of the grains of powder are comparable to the focal spot size (35μm).

Modeling the Temperature Fields of Copper Powder Melting in the Process of Selective Laser Melting

A model of the temperature fields was created and used to reduce the defect of excess melted particles on the lateral faces of the scanning area. By analyzing the temperature field during each stage of the scan, optimization of the pattern could be achieved to minimize the heat transferred to material outside of the scanning area. The study proposes that extended surfaces be divided into sub-areas and scanned separately to let the powder outside the scan area cool. Alternating

the direction of the can in each sub-area is also recommended. This technique aids the surface finish of the lateral faces of a SLM produced part.

MSDS Chromium (VI) Oxide

The sintering process that occurs inside the SLM produces a byproduct called Hexavalent Chromium, also known as Chromium VI, or Chromium 6. Human exposure to Chromium 6 is extremely detrimental to health. Chronic exposure is known to cause lung and gastrointestinal cancer as well as heritable genetic damage. Exposure can occur via inhalation of mists, dusts or fumes containing Chromium 6, or via contact with skin or eyes. Immediate effects of inhalation are severe irritation of the respiratory tract which could result in burning pain, coughing, shortness of breath, and pulmonary edema. Inhalation exposure can be fatal as a result of spasms. Prolonged exposure may result in systematic effects. Skin readily absorbs Chromium 6 and results in burns, skin sensitization, rash, deep ulcers. Contact with eyes will cause severe eye burns and may cause permanent corneal damage or other irreversible eye damage. Chromium 6 is also extremely toxic to aquatic animals and could cause long-term adverse effects in aquatic environments.

OSHA Chromium (VI) Oxide

Chromium 6 is any form or compound containing chromium with a positive six valence. The main form of exposure to Cr(VI) is from inhalation of airborne particles of Cr(VI). The permissible exposure limit (PEL) is 5 micrograms per cubic meter of air, which is determined as an 8-hour time-weighted average (TWA). Half of the permissible exposure limit indicates the 'action level.' The calculation of this 8-hour TWA is required by OSHA for each employee exposed to Cr(VI), using an adequate number of personal breathing zone samples to accurately determine exposure per person, on each shift, in each work area.

If initial monitoring indicates an exposure level below action level, monitoring may end if an independent test confirms the adequately low exposure level. If initial monitoring shows exposure levels above the action level, employers are required to monitor exposure levels every six months. If exposure levels are above the PEL, monitoring must occur quarterly. Periodic monitoring must occur whenever there is a change to process, material, personnel, or equipment. Employers must individually notify affected employees within fifteen work days of learning about exposure, or post results in a communal area accessible to all affected employees. If results are above PEL, a written notice of corrective action taken to reduce exposure to or below PEL must be given to employee.

An employer must establish and mark a regulated area wherever exposure to Cr(VI) can reasonably be expected to be found. Only employees with the proper training and work duties requiring access should be permitted to utilize theses areas. Employer must provide, at no cost to employee, necessary respiratory protection during periods necessary to installing feasible engineering work practice controls, during the maintenance or repair of said work practices, or where all feasible work practices are not sufficient in reducing exposure levels below the PEL. Wherever respirator use is required, an appropriate respiratory protection program must be implemented by the employer. If other forms of exposure are likely to be present, employer must provide, at no cost to employee, all necessary personal protective equipment and ensure that it is

used. All personal protective equipment must be stored in a change room which assures no cross contamination with street clothes. This equipment must be cleaned, maintained, and disposed of by the employer. Any cleaning methods that disperse Cr(VI) into the air are prohibited.

Disposal of Cr(VI) must be done in a sealed, impermeable containers and labeled in accordance to requirements set by the Hazard Communication Standard.

Employers must assure that employees can demonstrate knowledge of OSHA regulations and medical surveillance program procedures.

III. Design

The information provided in this section is the design for a materials development experiment on a SLM 125 HL machine. The information is primarily based on a example using a undeveloped copper alloy--Glen Research Copper 84. This aspect of design is interchangeable with any material to be developed on a SLM machine.

Our project is limited by a few machine-related aspects. Firstly, because of the size of our machine (SLM 125 HL), we are limited to a build size 125 x 125 x 75 mm. We are also limited by the machine single fiber laser we can only use one type of scan pattern. Our machine uses a stripe pattern, as opposed to bigger machines that have more lasers allowing for them to print with a "checkerboard" pattern.

What we are first going to be testing is if we will be able to achieve 99% density with the GRCop 84 alloy. On one build plate, we will be printing multiple "density cubes.". Also, we will be able to test different parameters on each density cube on the plate. Then, a fractional factorial D.O.E will test the different parameters' effects on the print density. The parameters to be tested are as follows:

- Scan speed
- Gas flow
- Laser power
- Pattern size
- Filter length
- Hatch Pattern
- Hatch distance
- Part orientation on build plate

Scan speed determines the speed of vectors in mm/s. Changing this parameter could lead to two negative results: one is that the scan speed would be too slow, accumulating too much heat at points causing warpage of part or heat affected zones. The other is that if the scan speed is too fast, there could be areas where powder is not fully melted, which could then not achieve the density goal.

Gas Flow is changed in the way of the angle it is oriented. Looking at the chamber of the SLM from the front, the gas will flow from left to right of the chamber. To change the angle of the gas flow, it must be specifically enabled in the Magics software. The angle will rotate the gas flow clockwise, which will change the direction that build and scanning orders are processed because they will be directed against the flow of the gas.

Laser power (Watts) effectively controls the material melt temperature. This will then influence the quality of our builds directly, in the sense that if the laser is at too high of a power, it will warp and possibly destroy the part. Though at too low of a temperature, the build will not be processed all the way, leaving material not bonded and porosities in the part.

Pattern size refers to the maximum length that the pattern can be. This also refers to the specific

STL vector lengths that are made into hatch lines on the part, and therefore the path that the laser will take. Pattern size will affect the accuracy of our parts, because a smaller pattern size could help to create much more accurate parts. Filter length is a filter that will eliminate vectors that are too short on parts, such that small features on parts will not get destroyed.

Hatch pattern is the determined offset vector that are used to fill the inner areas of parts. There are a few ways that the hatch pattern can be modified: the first way is with the hatch distance. This is the distance that the vectors are offset from each other. A second way is that the hatch pattern can be rotated. These two parameters, when adjusted, will aid in reaching our density objective.

We will place the geometrically similar parts (density cubes) (Figure 3-2). on the build plate in a row and column format. We will be able to test different parameters in the rows. and the values that we plan to test them at along the column. For example, in the SLM user manual, in the material development section, there is an example of this method (Figure 3-1). All parameters other than the one being tested will remain the same. There are many other parameters as far as part orientation that we can change. Changing the distance between the parts, which includes both the distance between the rows and the columns, can be beneficial in isolating the different parameter tests from each other. We can also change the line pulling, which effectively shifts each row and can help to distribute heat on the build plate, isolating our samples even more. Next is our angle of rotation: this allow us to rotate the matrix of parts on the build plate, which is another way that we can distribute the build plate heat. Lastly we can change the border width in the part orientation, which effectively helps to create a safety zone around the matrix.

Once we achieve our objective of 99% density we will move on to our other tests we will move to porosity. Porosity will be tested using the radio knobs (Figure 3-3). The method for testing porosity will be similar to the testing of the density cubes. The radio knobs are meant to mainly test if the changes of workpiece diameter have an effect on porosity. We will be using our best recipes from the density cubes to carry out this test. Our methods for inspecting the porosity will be further discussed in the methods section.

After porosity and density testing have been completed, we will work on the tensile bars. Due to our machine restriction of build, we are limited to the size tensile specimens we can use. Keeping this in mind we, will be using the standard size ASTM E8 subsize tensile specimens (Figure 3-4). Using our best defined recipes we will print these specimens in two different ways. One has bars being printed perpendicular to the plate, and the other will be parallel to the plate. This could result in a potential difference in the tensile strength of the specimens. It would then show us parts that are heavily reliant on tensile strength need to be printed in a certain orientation.

Another part that we will be producing to further validate our design is the klino cube (Figure 3-5). The klino cube's purpose is to test complex geometry. We will be measuring multiple aspects of the klino cube for dimensional accuracies, including surface roughness in multiple places on the cube. The klino cube's base dimensions are roughly 2.5 x 5 x 2.5 cm. A more detailed breakdown of the dimensions will be given in the methods section.

The final validation of our recipe will be the residual stress comb (Figure 3-6). Its purpose is to show if our recipe leaves any stresses within our parts. If the comb has any internal residual stresses, it will either pull away from the support material, bend, or break. It will over heat in certain places, causing visible warpage. If any of these issues occur we will have to further refine our recipe.

IV. Methodology

To explain our testing methods, we will use data that we have found on Glen Research copper 84. This can serve as a case study that can be used as a reference to test any material that will be developed on an SLM.

We will be testing the density of cubes by comparing their experimental masses to theoretical masses. Also, we will be completing a visual inspection of the part. NASA Aerospace Structural Materials Handbook Supplement GRCop-84 states the room temperature density of GRCop-84 with a 95% confidence interval is 8.62 +/- 0.08 g/cm^3. We will produce 5 mm cubes so our theoretical mass will range between 106.75 and 108.75 g. To visually inspect the parts, we will cut them in half and under magnification, look for voids and other defects. This would indicate why we may have not achieved our density objective. The porosity testing with the radio knobs will be done by cutting radio knobs in half and inspecting them under magnification to see if there are porosities

The testing of tensile specimens will be done using an Instron 5969 in the Cal Poly Aerospace structures lab. Since there will be parts produced in two orientations on the build plate we will be comparing multiple samples of each orientation to see if this has an effect on the tensile strength. Tensile strength will be compared to extruded GRCop-84 data (Figure 4-2) courtesy of the NASA Aerospace Structural Materials Handbook Supplement GRCop-84. The klino cube surface roughness is expected to be in the 10-30 micron range on the top surface primarily. We will measure multiple features on the Klinocube all dimensions to be measured are shown in the klinocube drawing, these can be seen in (Figure 4-1). The residual stress comb will be mainly inspected visually. As it will be printed with our best recipes and upon it cooling if it has pulled away from the build plate or fractured in any places it will be indicative of residual stresses.

V. Results

Materials Development

I. Full Factorial design

To start a materials development on any material the first step is to create a full factorial design with the three parameters that are the most correlated with density: scan speed, laser power, and hatch distance. These parameters will be varied between a low and a high setting creating 16 parts. As seen in Figure 5-1 these parameters were chosen for 316 Stainless steel, but can be changed for any application. The power density is also included in Figure 5-1, which shows the correlation of parameters to each other. Samples that have the same power density will most likely have the same actual density. These values will be applied to 16 density cubes on a build plate and printed.

II. Collect Data

After the parts have been printed and post-processed (removed from build plate and polished), the parts will be weighed and measured. this mass and volume is to be recorded and to find density.

III. Analysis of Data

Once density has been collected, an analysis using a statistical software (JMP, minitab, etc.) will be conducted and the parameters that correlate the most to density will be identified. These parameters will then be recorded for the next step.

IV. Incremental Experiment

After the analysis is completed, the next step is to do an incremental experiment with the density cubes. The factor that is the most correlated to density will be varied incrementally from the low to high value in the full factorial experiment, while other parameters are held constant (Figure 5-2).

V. Analyze Final Results

Post processing and inspection are then conducted on the incremental experiment's density cubes. The cube with the highest density will be selected for the recipe.

VI. Manufacture Additional Parts/Testing of Parts

Using the recipe determined during the incremental experiment, radio knobs, tensile specimens, klinocubes, and residual strength combs will be produced. See *Methods* section for testing protocol on these parts.

Safety Results

Due to Environmental Health and Safety (EH&S) findings, Cal Poly is currently unable to utilize the SLM printers. After speaking with industry experts at the University of Louisville, we have learned that the following personal protective equipment (PPE) must be purchased: ESD lab coat, ESD boots, nitrile gloves, particle size counter, PAPR full face respirator system, totalling about $2000.

Beside PPE, dedicated post-processing equipment is necessary, as Chromium 6 is present in the part and build plate. The post-processing equipment needed include: bandsaw, grinder/sander, shop vacuum, and carboys for coolant, totalling about $2600. This equipment must be stored with the SLM printers, or in a room that is monitored for Chromium 6 concentration in compliance with OSHA standards (see OSHA standard number 1910.1126).

New post-processing procedures must be developed for the tasks of part removal from build plate and coolant disposal. The coolant from the bandsaw contains high concentrations of Chromium 6, which is also extremely toxic to aquatic environments. Proper disposal using sealed carboys is needed to ensure the safety of the operators and the environment. The dust from grinding or sanding must be cleaned in a way that does not make the dust aerosolized.

Only individuals who have completed the appropriate training may have access to the SLM printers. Professors and lab supervisors are to attend an additive manufacturing metal powder safe training at the University of Louisville this summer. Training may be offered to select students at staff discretion.

Economic Results

For our economic analysis, we chose a copper nozzle (Figures 5-1 and 5-2). It can be machined using a CNC lathe and CNC mill, thus we are comparing the cost of machining the nozzle versus the cost of using SLM to build it.

We began by calculating the cost per part of both alternatives. It takes significantly less time to produce a part via CNC machining. However, a CNC operator costs more per hour and is required to monitor the entire length of the process. Very little monitoring of the SLM process is required, meaning that it is not necessary to pay an operator for the entire length of the build. Cost per part was calculated using DFM Concurrent Costing 2.4, and by using expert estimations of SLM build time. The cost per part of the CNC process was $608.01, and $146.50 for the SLM. Due to the labor difference, we found that using the SLM was $461.51 less per part than CNC machining.

The initial investment for a SLM printer is around $300,000 while for both a CNC mill and CNC lathe is around $150,000. The CNC process also produces parts faster than the SLM, 1.25 parts per shift vs 1 part per shift from the SLM (assuming an eight hour shift per day, and 80% factory

utilization). However, due to the drastic difference in cost per part, the SLM process is the better investment. Assuming sale cost of $750 per nozzle, we analyzed both processes and found their internal rate of return and net present value after five years, assuming a 10% discount rate.

	Internal Rate of Return (IRR)	Net Present Value (NPV)	Payback period
SLM	38.96%	$249,057.56	2.07
CNC Machining	13.473%	$161,476.15	3.47

Table 5-1: Economic comparison of CNC and SLM processes

The above calculation results (Table 5-1) show that while the SLM has a significantly higher initial investment, the lower cost per part means that the IRR and NPV of the SLM is higher after five years of operation. The payback period is also a year shorter than the CNC machining alternative.

VI. Discussion

Our project faced significant delays because of safety issues surrounding the SLM printers. Use of these printers was prohibited due to EH&S concerns. These delays forced us to change the scope of our project away from a specific metal powder, towards a more general materials development design.

These safety concerns also prevented the completion of a contract with a company sponsor that was to provide Glenn Research Copper-84 powder for testing purposes.

The lack of GRCop-84 powder and use of the SLM printers meant that we had to consider alternative designs. Before use of the SLM was prohibited, we considered using a generic material instead of GRCop-84. After the SLMs were shut down, we designed a materials development process that can be applied to any metal powder in an SLM.

Once Cal Poly acquires the necessary equipment and procedures, use of the SLM can resume. To continue this project, metal powders should be acquired so the procedure can be validated.

VII. Conclusions

Overall, the materials development module provided by SLM was not sufficient for production use. Because of unforeseen safety issues considering Chromium 6 in the SLM, we were not able to test parameters to determine a full parameters recipe. A materials development procedure with an experimental design is needed to establish a recipe of parameter values for each metal powder in production. With aid from research and expert advice, we developed a theoretical materials development module encompassing the following:

- A procedure that could generate a combination of parameter values that yield parts of 99% density or greater within 64 parts or 4 builds total.
- Testing methodology to fine tune parameters that affect warpage, surface finish, dimensional accuracy, and residual stresses.
- Evidence of the SLM process economic viability.
- Proof of importance of dedicated safety equipment and training for the SLM process.

Due to the safety concerns discussed, validation of the procedure was not moved past the theoretical state. Thus, the next step to complete this project is validation of the procedure. This can be accomplished as soon as the necessary safety equipment is purchased and procedures are put into place.

Appendix A. Figures

Figure 3-1 Density cube row matrix format

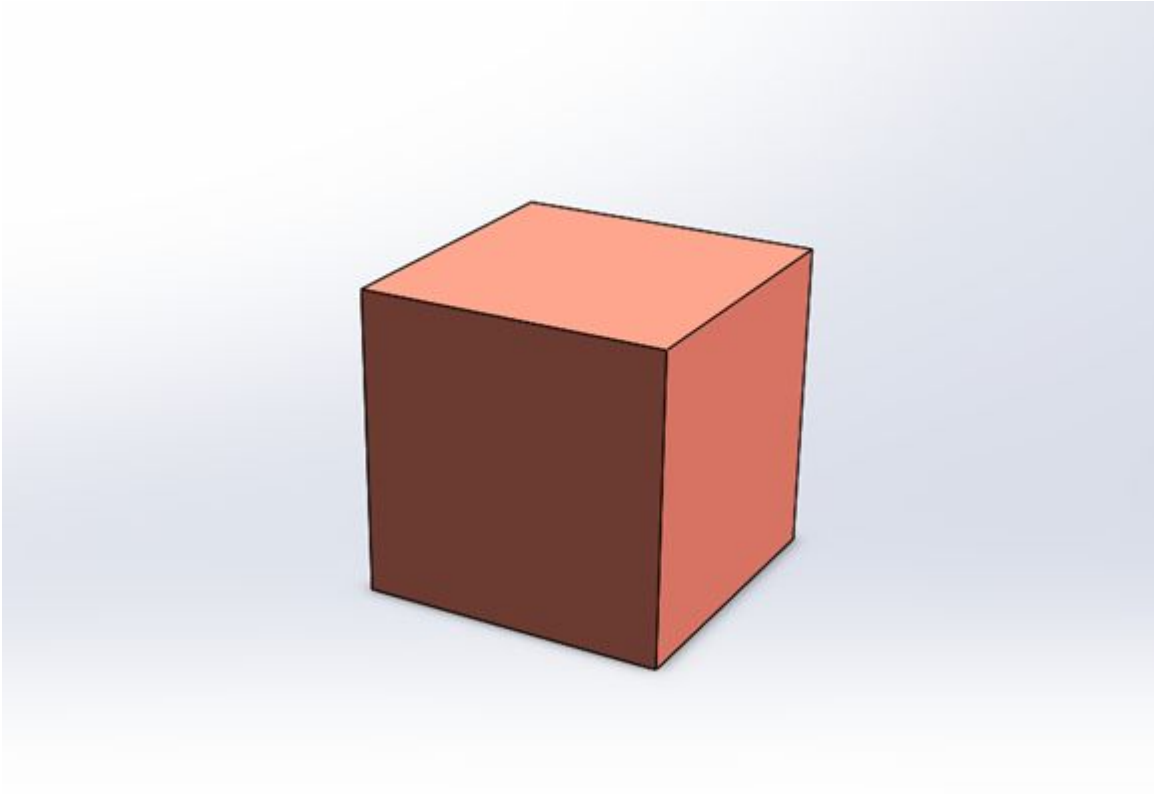

Figure 3-2 Density cube

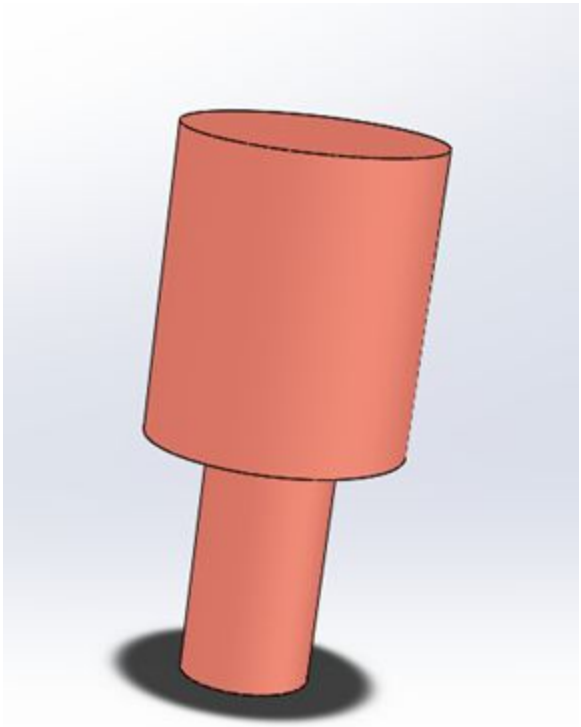

Figure 3-3 Radio knob

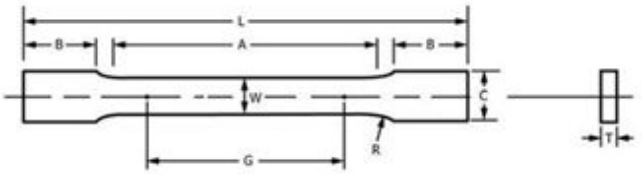

	Dimensions		
	Standard Specimens		Subsize Specimen
	Plate-Type, 40 mm [1.500 in.] Wide	Sheet-Type, 12.5 mm [0.500 in.] Wide	6 mm [0.250 in.] Wide
	mm [in.]	mm [in.]	mm [in.]
G—Gauge length (Note 1 and Note 2)	200.0 ± 0.2 [8.00 ± 0.01]	50.0 ± 0.1 [2.000 ± 0.005]	25.0 ± 0.1 [1.000 ± 0.003]
W—Width (Note 3 and Note 4)	40.0 ± 2.0 [1.500 ± 0.125, -0.250]	12.5 ± 0.2 [0.500 ± 0.010]	6.0 ± 0.1 [0.250 ± 0.005]
T—Thickness (Note 5)		thickness of material	
R—Radius of fillet, min (Note 6)	25 [1]	12.5 [0.500]	6 [0.250]
L—Overall length, min (Note 2, Note 7, and Note 8)	450 [18]	200 [8]	100 [4]
A—Length of reduced parallel section, min	225 [9]	57 [2.25]	32 [1.25]
B—Length of grip section, min (Note 9)	75 [3]	50 [2]	30 [1.25]
C—Width of grip section, approximate (Note 4 and Note 9)	50 [2]	20 [0.750]	10 [0.375]

Figure 3-4 ASTM E8 sub-size tensile specimen

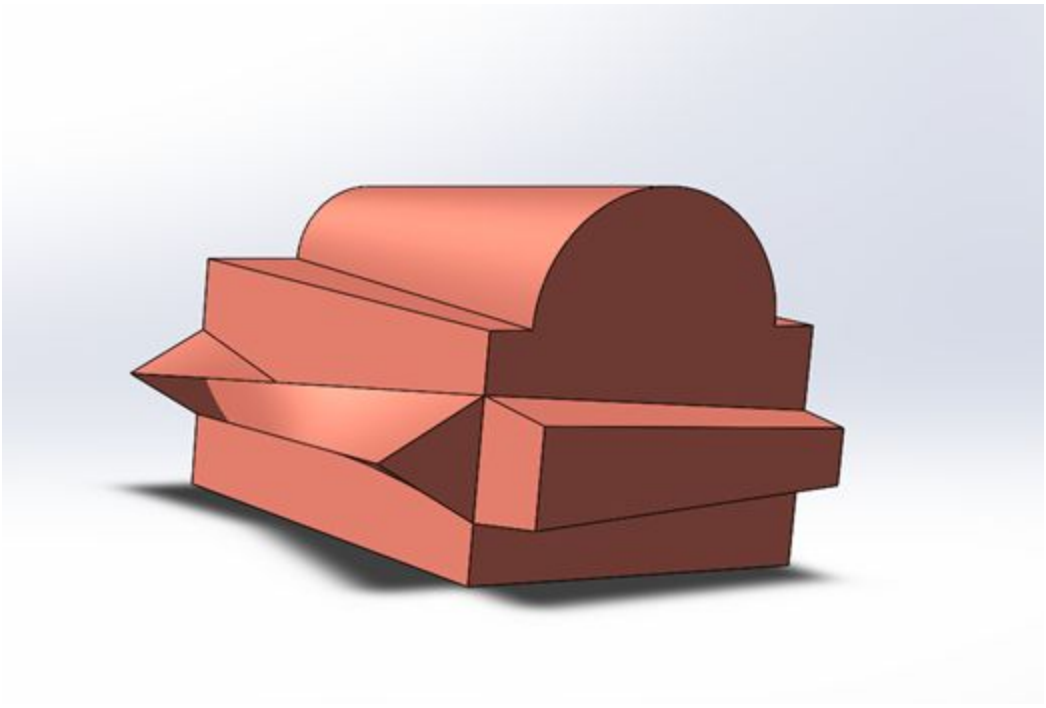

Figure 3-5 Klinocube Model

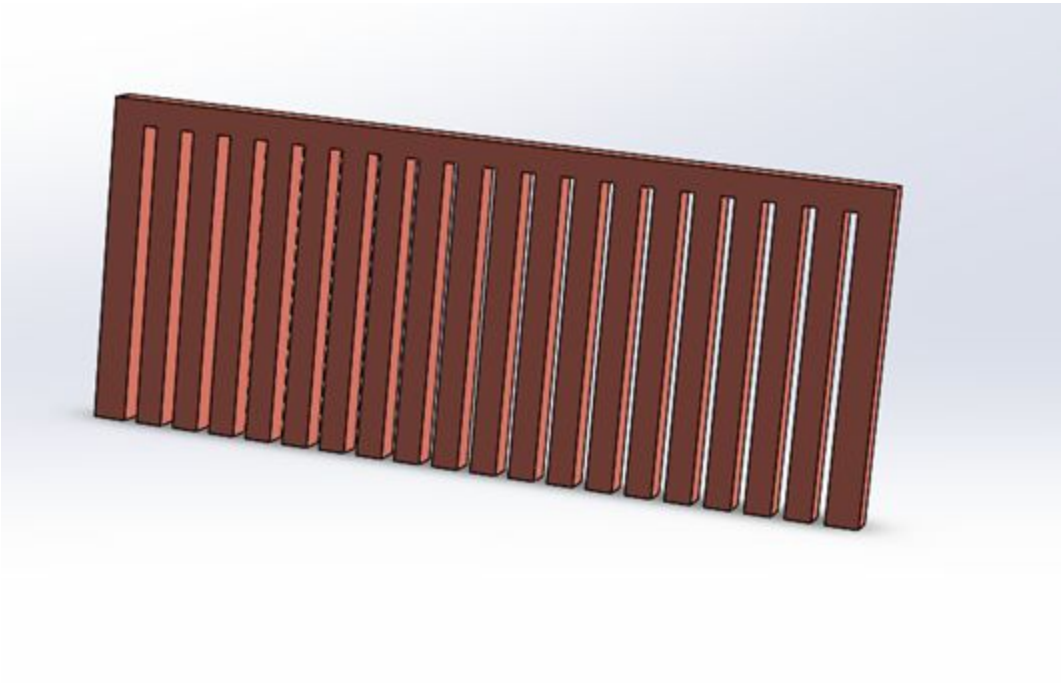

Figure 3-6 Residual stress comb

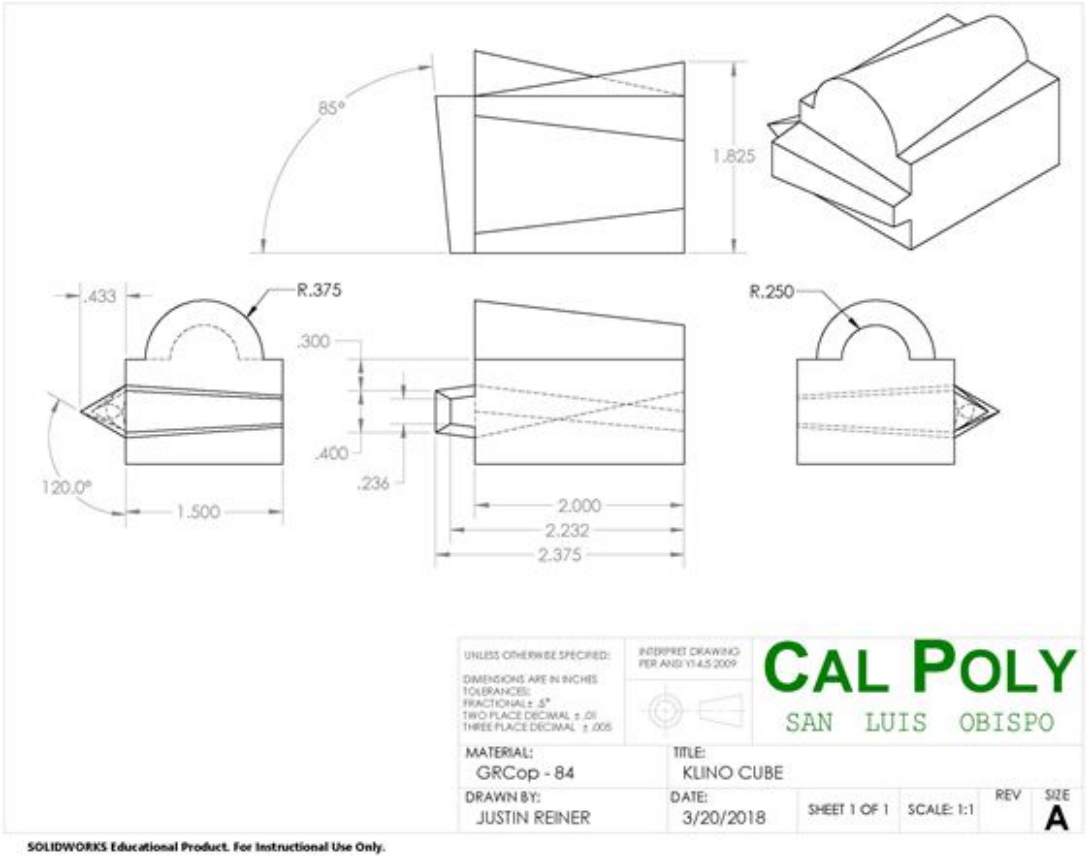

Figure 4-1 Klinocube drawing

Extruded:

$$\sigma_{0.2\%Offset}(T) = 297.4 - 0.312\,T + 3.175\times10^{-4}\,T^2 - 2.506\times10^{-7}\,T^3 - t(1-\alpha,31)\times10.92$$

HIPed:

$$\sigma_{0.2\%Offset}(T) = 155.3 + 6.86\times10^{-2}\,T - 1.70\times10^{-4}\,T^2 - t(1-\alpha,19)\times10.93$$

where T is in Kelvin, $t(1-\alpha, \nu)$ is the value for the t-distribution with ν degrees of freedom associated with $1-\alpha$ cumulative probability, and $\sigma_{0.2\%\,Offset}(T)$ is in MPa. Adjusting the value of $t(1-\alpha, \nu)$ allows calculation of differing confidence limits and both one and two sided confidence intervals. The regression models and lower 95% confidence intervals are shown in Figures 3.3.1.2-3.

3.3.1.2 [Figure] 0.2% offset yield strength of as-extruded GRCop-84

3.3.1.3 [Figure] 0.2% offset yield strength of as-HIPed GRCop-84

Ultimate tensile strength. The lower confidence interval for the ultimate tensile strength of GRCop-84 is given by the equations

Extruded:

$$\sigma_{UTS}(T) = 664.5 - 0.987\,T + 3.850\times10^{-4}\,T^2 - t(1-\alpha,32)\times21.92$$

HIPed:

$$\sigma_{UTS}(T) = 454.4 - 0.420\,T + 3.33\times10^{-5}\,T^2 - t(1-\alpha,19)\times30.70$$

where T is in Kelvin, $t(1-\alpha, \nu)$ is the value for the t-distribution with ν degrees of freedom associated with $1-\alpha$ cumulative probability, and $\sigma_{UTS}(T)$ is in MPa. The regression models and lower 95% confidence intervals are shown in Figures 3.3.1.4-5.

3.3.1.4 [Figure] Ultimate tensile strength of as-extruded GRCop-84

3.3.1.5 [Figure] Ultimate tensile strength of as-HIPed GRCop-84

Elongation. The lower confidence interval of the elongation of GRCop-84 is given by the equations

Extruded:

$$\varepsilon(T) = 17.16 + 0.034\,T - 8.114\times10^{-5}\,T^2 + 4.907\times10^{-8}\,T^3 - t(1-\alpha,31)\times2.52$$

HIPed:

$$\varepsilon(T) = -17.94 + 0.209\,T - 3.28\times10^{-4}\,T^2 + 1.43\times10^{-7}\,T^3 - t(1-\alpha,19)\times4.55$$

where T is in Kelvin, $t(1-\alpha, \nu)$ is the value for the t-distribution with ν degrees of freedom associated with $1-\alpha$ cumulative probability, and $\varepsilon(T)$ is in percent. The regression models and the lower 95% confidence intervals are shown in Figures 3.3.1.6-7.

3.3.1.6 [Figure] Elongation of as-extruded GRCop-84

3.3.1.7 [Figure] Elongation of as-HIPed GRCop-84

Reduction in area. The lower confidence interval for the reduction in area of GRCop-84 is given by the equations

Extruded:

$$RA(T) = 5.73 + 0.239\,T - 4.183\times10^{-4}\,T^2 + 1.956\times10^{-7}\,T^3 - t(1-\alpha,31)\times12.32$$

HIPed:

$$RA(T) = -96.92 + 0.763\,T - 1.23\times10^{-3}\,T^2 + 5.88\times10^{-7}\,T^3 - t(1-\alpha,19)\times11.65$$

where T is in Kelvin, $t(1-\alpha, \nu)$ is the value for the t-distribution with ν degrees of freedom associated with $1-\alpha$ cumulative probability, and RA(T) is in percent. The regression models and the lower 95% confidence intervals are shown in Figures 3.3.1.8-9.

3.3.1.8 [Figure] Elongation of as-extruded GRCop-84

3.3.1.9 [Figure] Elongation of as-HIPed GRCop-84

Figure 4-2 NASA Aerospace Structural Materials Handbook Supplement GRCop-84 extruded tensile strength section

Pattern	Power (W)	Speed (m/s)	Hatch Distance (mm)	Density	Power Absorbtion
−−−	50	2	0.15	•	166.66666667
−+−	50	8	0.15	•	41.666666667
+++	300	8	0.5	•	75
+++	300	8	0.5	•	75
+−+	300	2	0.5	•	300
+−+	300	2	0.5	•	300
−−+	50	2	0.5	•	50
+−−	300	2	0.15	•	1000
−−−	50	2	0.15	•	166.66666667
++−	300	8	0.15	•	250
+−−	300	2	0.15	•	1000
++−	300	8	0.15	•	250
−+−	50	8	0.15	•	41.666666667
−++	50	8	0.5	•	12.5
−−+	50	2	0.5	•	50
−++	50	8	0.5	•	12.5

Figure 5-1 Full factorial experiment design

Part Number	Hatch Distance (mm)	Power (W)	Speed (m/s)	Density (g/ cm^3)
1	0.15	300	8	•
2	0.2	300	8	•
3	0.25	300	8	•
4	0.3	300	8	•
5	0.35	300	8	•
6	0.4	300	8	•
7	0.45	300	8	•
8	0.5	300	8	•

Figure 5-2 incremental experiment design

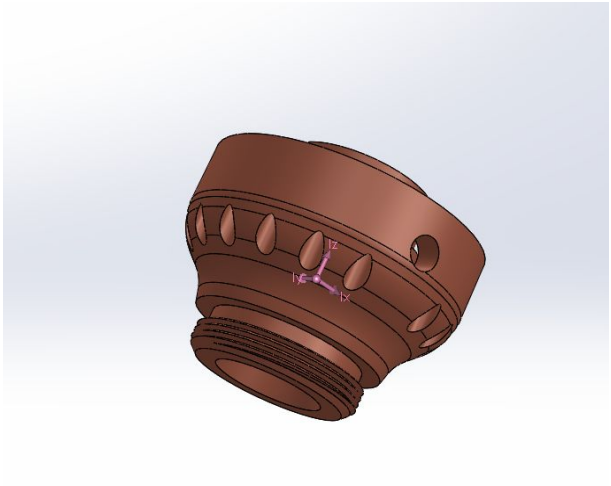

Figure 5-3 Copper nozzle for economic analysis

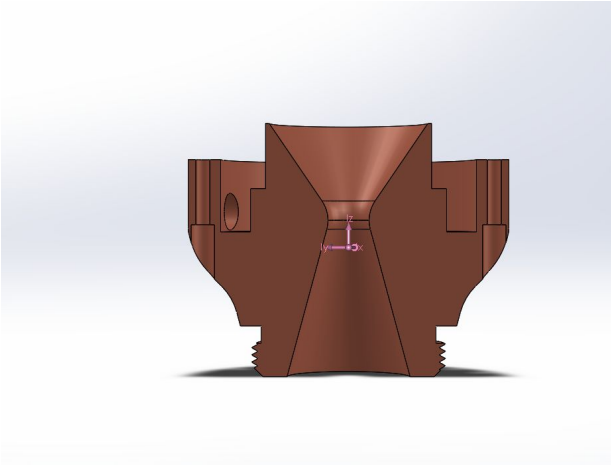

Figure 5-4 Section view of copper nozzle

References

Huang, Runze. “Environmental and Economic Implications of Distributed Additive Manufacturing.” *Journal of Industrial Ecology*, Wiley Periodicals, Inc., 2017, https:/reiner/www-sciencedirect-com.ezproxy.lib.calpoly.edu/science/article/pii/S0925527315000547.

Weller, Christian, et al. “Economic Implications of 3D Printing: Market Structure Models in Light of Additive Manufacturing Revisited.” *Science Direct*, International Journal of Production Economics, June 2015, www-sciencedirect-com.ezproxy.lib.calpoly.edu/science/article/pii/S0925527315000547.

Ellis, David L, and Bradley A Lerch. “Improvement of GRCop-84 Through the Addition of Zircounum .” *NASA Technical Reports Server*, NASA, June 2012, drive.google.com/open?id=13IwAx8xr76vBsIJB9vksym0xZScZt-qE.

Raus, A A. “The Influence of Selective Laser Melting Parameters on Density and Mechanical Properties of AlSi10Mg.” *MATEC Web of Conferences 78*, EDP Services, 2016, drive.google.com/open?id=1bpwvUCRX6_IhxLnc9k-rAMvR7GXZu_Pz.

Diegel, Olaf. *Tools for Sustainable Product Design: Additive Manufacturing*. Journal of Sustainable Development, Sept. 2010, drive.google.com/open?id=1rT9plEasHuxyQdSepGUFYXehTfJ3eR-Z.

Atzeni, Eleonora, and Alessandro Selmi. “Economics of Additive Manufacturing for End-Usable Metal Parts.” *Int J Advanced Manufacturing Technology*, Springer-Verlage London Limited, 2012. https://drive.google.com/open?id=1dU11AD5A8r2M5KX3DFsIDNu1dxugJ0wD

Decker, M W, et al. “Creep Properties of an Extruded Copper-8% Chromium-4% Niobium Alloy.” *Materials Science and Engineering*, Elsevier, 20 Oct. 2003, drive.google.com/open?id=1sSbxkoDKnuYMfN3q4tkkLGUIqGa8Lq9n.

De Groh, Henry C, et al. “Comparison of GRCop-84 to Other Cu Alloys with High Thermal Conductivities.” *NASA Technical Reports Server*, NASA, 1 Jan. 2007, drive.google.com/open?id=1waG1r_W79VU6aTiD70AP6BR4I_ma4zfI.

Ellis, David L. “GRCop-84: A High-Temperature Copper Alloy for High-Heat-Flux Applications.”*NASA Technical Reports Server*, NASA, 1 Feb. 2005, drive.google.com/open?id=1dpiGsnb8VqyetuthJPQl4YGg27fTLmRB.

Gong, Haijun. *The Effects of Processing Parameters on Defect Regularity in Ti-6Al-4V Parts Fabricated By Selective Laser Melting and Electron Beam Melting* . University of Louisville, Kentucky, 16 Aug. 2013, sffsymposium.engr.utexas.edu/Manuscripts/2013/2013-33-Gong.pdf.

Buchmayr, Bruno. “Laser Powder Bed Fusion - Materials Issues and Optimized Processing Parameters for Tool Steels, AlSiMg - and CuCrZr Alloys.” *Advanced Engineering Materials*, Rapid, 2017, drive.google.com/open?id=17y9gVsiUV5o12lM4EjW3THDdtIrdH9xN.

Lane, Brandon, et al. “Multiple Sensor Detection of Process Phenomena in Laser Powder Bed Fusion.” *Proceedings of SPIE*, National Institute of Standards and Technology, 11 May 2016, drive.google.com/open?id=14r-bZyzpFsLWR1VaGgavb5jPIMHouARC.

King, W. “Overview of Modelling and Simulation of Metal Powder Bed Fusion Process at Lawrence Livermore National Library.” *Materials Science and Technology*, Taylor & Francis, 2015, drive.google.com/open?id=12Wg3wxKWyqM-E741QgCPfnrrTQKOQlAz.

Grasso, Marco, and Bianca Maria Colosimo. “Process Defects and In Situ Monitoring Methods in Metal Powder Bed Fusion: A Review.” *Measurement Science and Technology*, IOP Publishing, 15 Feb. 2017, drive.google.com/open?id=1RhwaX_3gGQlgqYIzSruL8a2BMQTDGH1L.

Jhong, Kai Jyun. “Microstructure and Magnetic Properties of Magnetic Material Fabricated by Selective Laser Melting.” Physics Procedia., vol. 83, 2016, pp. 818–824. https://ac-els-cdn-com.ezproxy.lib.calpoly.edu/S1875389216301912/1-s2.0-S1875389216301912-main.pdf?_tid=dadbc5c6-cf8d-4f0b-aa62-1cdc652796b0&acdnat=1521427373_ba2d6781d3e84dacf611f8a0e759e3fc

Kaden, Lisa. “Selective Laser Melting of Copper Using Ultrashort Laser Pulses.” Applied Physics., vol. 123, no. 9, 2017, pp. Applied physics. , 2017, Vol.123(9). https://link-springer-com.ezproxy.lib.calpoly.edu/article/10.1007%2Fs00339-017-1189-6

Leordean, Dan. “Customized Implants with Specific Properties, Made by Selective Laser Melting.” Rapid Prototyping Journal., vol. 21, no. 1, 2015, pp. 98–104. https://search-proquest-com.ezproxy.lib.calpoly.edu/docview/1647138547?accountid=10362

Rickenbacher, L. “An Integrated Cost-Model for Selective Laser Melting (SLM).” Rapid Prototyping Journal., vol. 19, no. 3, 2013, pp. 208–214. https://www-emeraldinsight-com.ezproxy.lib.calpoly.edu/doi/full/10.1108/13552541311312201

Saprykin. “Modeling the Temperature Fields of Copper Powder Melting in the Process of Selective Laser Melting.” IOP Conference Series. Materials Science and Engineering / Institute of Physics., vol. 142, no. 1, pp. IOP conference series. Materials science and engineering / Institute of Physics. , Vol.142(1). http://iopscience.iop.org/article/10.1088/1757-899X/142/1/012061/pdf

Yap, C.Y., et al. “Review of Selective Laser Melting: Materials and Applications.” Applied Physics Reviews., vol. 2, no. 4, 2015, p. 041101. https://aip-scitation-org.ezproxy.lib.calpoly.edu/doi/10.1063/1.4935926

MSDS# 95984 Chromium(VI) Oxide http://www.clayton.edu/portals/690/chemistry/inventory/MSDS%20chromium(VI)%20oxide.pdf

OSHA standard number 1910.1126, Chromium (VI).
https://www.osha.gov/pls/oshaweb/owadisp.show_document?p_table=standards&p_id=13117